TRANSIT-TIME DEVICES AS LOCAL OSCILLATORS FOR FREQUENCIES ABOVE 100 GHz *)

H. Eisele, C. Kidner, G. I. Haddad

Center for Space Terahertz Technology
Department of Electrical Engineering & Computer Science
2231 EECS Building
The University of Michigan
Ann Arbor, Michigan 48109-2122

Abstract:

Very promising preliminary experimental results have been obtained from GaAs IMPATT diodes at F-band frequencies (75 mW, 3.5 % @ 111.1 GHz and 20 mW, 1.4 % @ 120.6 GHz) and from GaAs TUNNETT diodes at W-band frequencies (26 mW, 1.6 % @ 87.2 GHz and 32 mW, 2.6 % @ 93.5 GHz). These results indicate that IMPATT, MITATT and TUNNETT diodes have the highest potential of delivering significant amounts of power at Terahertz frequencies. As shown recently, the noise performance of GaAs W-band IMPATT diodes can compete with that of Gunn devices. Since TUNNETT diodes take advantage of the quieter tunnel injection, they are expected to be especially suited for low-noise local oscillators. This paper will focus on the two different design principles for IMPATT and TUNNETT diodes, the material parameters involved in the design and some aspects of the present device technology. Single-drift flat-profile GaAs D-band IMPATT diodes had oscillations up to 129 GHz with 9 mW, 0.9 % @ 128.4 GHz. Single-drift GaAs TUNNETT diodes had oscillations up to 112.5 GHz with 16 mW and output power levels up to 33 mW and efficiencies up to 3.4 % around 102 GHz. These results are the best reported so far from GaAs IMPATT and TUNNETT diodes.

---

*) This work was supported by NASA under contract No. NAGW 1334.

1. Introduction

GaAs IMPact ionization Avalanche Transit-Time (IMPATT) diodes have long been thought to be limited to frequencies below 60 GHz. Little has been reported regarding the operation of GaAs IMPATT or MITATT diodes above 100 GHz [1,2]. Experimental results of W-band IMPATT diodes (up to 320 mW, 6.0 % @ 95 GHz) [3] with excellent noise performance [4] clearly indicate that IMPATT diodes are one prime candidate to fulfill the growing need for local oscillators above 100 GHz. TUNNEl injection Transit-Time (TUNNETT) diodes were already proposed in 1958 and are considered another prime candidate for low-noise, medium power sources at millimeter and submillimeter frequencies. Although pulsed oscillations were demonstrated up to 338 GHz in 1979 [5], CW power has only recently been obtained from devices with low impact ionization carrier multiplication [6]. This significant progress is mainly due to the fact that refined epitaxial growth techniques have become widely available. Despite the impressive progress in oscillators with three-terminal devices at mm-wave frequencies [7] two-terminal devices hold the highest potential in delivering significant amounts of power with clean spectra above 100 GHz.

2. Design of single-drift flat-profile IMPATT diodes

In GaAs, the first derivative of the ionization rates of electrons and holes with respect to the electric field saturates around 500 $kVcm^{-1}$ [8-10]. Together with dead space effects in the avalanche zone [11] this saturation phenomenon favors a flat-profile structure for frequencies above V-band (50 - 75 GHz). The performance of a single-drift structure is the least sensitive to doping profile variations. The design of this structure is based on the assumption that the center of the avalanche region occurs where the electron concentration equals the hole concentration for the applied bias voltage [12] and that such a defined avalanche region is electrically equivalent to an avalanche region of the same width l_a but constant electric field and ionization rates [10]. The drift region - where ionization is to be neglected - is defined in its length l_d by the maximum in the well known transit-time function [13]

$$l_d = \frac{3\, v_s}{8 f_o} \quad , \tag{1}$$

where v_s is the average saturated drift velocity (4.5×10^6 cms^{-1} in GaAs for T_j = 500 K) [9,10] and f_o the operating frequency. Several structures for operating frequencies between 130 GHz and 160 GHz have been designed and the nominal doping profile of such a $p^{++}nn^+$ structure is given in Figure 1. A bias current density J_{DC} of 60 $kAcm^{-2}$ extrapolated from the experimental results in W-band [3] was taken into account.

3. Design of single-drift TUNNETT diodes

The design of the TUNNETT diode structure is based on a first order large signal theory [14] and experimental studies of highly doped MBE grown $p^{++}n^{+}$ structures. The carrier generation rate due to tunneling does not depend on the current density, but does strongly depend on the electric field. Therefore, a sharp pulse of electrons is injected at the $p^{++}n^{+}$ junction when the RF field reaches its maximum.

Under these assumptions for the $p^{++}n^{+}nn^{+}$ structure the first order large signal theory predicts a maximum in RF output power and DC to RF conversion efficiency [13,14] for

$$l_i + l_d = \frac{5\, v_s}{7 f_o} \quad , \tag{2}$$

where l_i is the length of the n^{+} region in the $p^{++}n^{+}$ junction, l_d is the length of the n region, v_s is the average saturated drift velocity (4.6×10^6 cms^{-1} for T_j = 500 K) [9,15] and f_o the operating frequency. Since the design is based on considerably lower electric fields in the drift region compared to the ones in the IMPATT diodes above, a slightly higher value for v_s is appropriate. Further details of the design procedure are given in References 16 and 17. The carrier concentration due to a current density J_{DC} of 25 kAcm^{-2} is taken into account in the doping profile. The nominal doping profile of this $p^{++}n^{+}nn^{+}$ TUNNETT diode structure is depicted in Figure 2.

4. Device technology

The operating current density of 60 kAcm^{-2} in a single-drift flat-profile GaAs D-band IMPATT diode requires a diamond heat sink to keep the operating junction temperature below 250 °C. Therefore all IMPATT diodes were fabricated using a well established selective etching technology for substrateless diodes on diamond heat sinks which gives up to 600 diodes per cm^2 wafer area with high uniformity [18]. This technology implements an $Al_{.55}Ga_{.45}As$ etch-stop layer between the substrate and the epitaxial layers for the device. In order to get the steep transitions for doping profiles in the submicron range, all wafers were grown by MBE. Figure 3 shows the flow chart of this technology process. The epitaxial side of the wafer is metallized with Ti/Pt/Au for a p^{+} ohmic contact, then selectively plated with gold to form a grating for mechanical support and glued on a ceramic carrier. In the next step the substrate is removed by selective wet chemical etch and subsequently the etch-stop layer in another selective wet chemical etch. A Ni/Ge/Au contact metallization is evaporated on top of the n^{+} layer and plated with gold to ease bonding. Contact patterns and diode mesas are defined by standard positive photoresist technology and wet chemical etching. The diodes outside the supporting grating are tested and selected for good DC characteristics

and thermocompression bonded on diamond heat sinks which are embedded in plated copper blocks. Electrical contact to the diode is provided by four metallized quartz stand-offs thermocompression bonded onto the heat sink and tapered gold ribbons bonded on the diode and the stand-offs.

The TUNNETT diodes were designed to operate at a maximum current density of 25 $kAcm^{-2}$ and a DC bias voltage comparable to the one of the IMPATT diodes. This allows fabrication of TUNNETT diodes with an integral heat sink. The wet chemical etching in the previously described technology limits the choice of materials and the minimum diameter for the n^+ ohmic contact. Therefore a different process has been developed, which likewise implements an $Al_{.55}Ga_{.45}As$ etch-stop layer between the substrate and the epitaxial layers for the device. Its flow chart is given in Figure 4 and further details are discussed in Reference 19.

Before the epitaxial side of the MBE-grown wafer is metallized with Ti/Pt/Au for a p^+ ohmic contact, grooves are selectively etched down to the AlGaAs etch-stop layer to divide the device layers into square shaped islands. This reduces the stress in the device layers during annealing. Furthermore, it shapes the Ti/Pt/Au layers and the plated gold layer of the integral heat sink thus providing additional mechanical strength for the subsequent processing steps after the substrate has been removed. The contacts are defined by standard lift-off technology and an additional metallization and photolithography step gives holes on top of the n^+ ohmic contact through which up to 3 µm of gold is electroplated. The mesas are formed by a wet chemical etch. After annealing the sample is diced into individual diodes and diodes with the desired size and DC characteristic are soldered or glued to a gold plated copper block. Electrical contact to the diode is provided by four metallized quartz stand-offs thermocompression bonded onto the plated block and tapered gold ribbons bonded on the diode and the stand-offs.

5. Experimental results

RF testing is performed in full height waveguide cavities with a resonant cap on top of the diode. IMPATT diodes are tested both in W-band (WR-10 waveguide) and D-band (WR-6 waveguide). TUNNETT diodes are only tested in W-band.

Figure 5 shows RF output power, DC to RF conversion efficiency and oscillation frequency of the best IMPATT diode in a W-band cavity as a function of the bias current. At each bias point the short plunger of the cavity and at some bias points also the E-H-tuner were adjusted for maximum output power. As can be seen from Figure 5, the efficiency reaches its maximum of 3.8 % at an output power of 72 mW.

An output power of 85 mW at 102.0 GHz with an efficiency of 2.5 % in WR-10 waveguide cavity and 20 mW at 120.6 GHz with an efficiency of 1.4 % in a WR-10 waveguide cavity were obtained from other

IMPATT diodes. The highest oscillation frequency of 128.4 GHz could be observed in a WR-6 waveguide cavity. At this frequency the output power was 9 mW and the efficiency 0.9 %. Table 1 summarizes the experimental results obtained from these diodes. The operating junction temperature was limited up to $T_j = 550$ K in order to ensure reliable long-term operation.

Frequency [GHz]	102.0	111.1	111.5	120.6	128.4
Output power [mW]	85	75	48	20	9
Efficiency [%]	2.5	3.5	2.3	1.4	0.9
Cavity (W/D)	W	W	W	D	D

Table 1: Experimental results of IMPATT diodes in W-band and D-band cavities.

To verify the mode of operation the DC I-V characteristics are measured at room temperature ($T = 300$ K) and an elevated temperature ($T = 370$ K). As shown in Figure 6a for low bias currents and Figure 6b for high bias currents, the breakdown of the D-band IMPATT diode is sharp and the bias voltage always increases with increasing temperature due to the decreasing ionization rates. The breakdown voltage at $T = 300$ K agrees well with breakdown voltages that were calculated from ionization rates evaluated in Reference 9, and which are plotted in Figure 7 together with the peak electric field strength. The sharp breakdown also proves that tunneling is significant only for electric field strengths above 1.0 $MVcm^{-1}$.

Figure 8 shows RF output power, DC to RF conversion efficiency and oscillation frequency of two TUNNETT diodes in W-band cavities as a function of the bias current. At each bias point the short plunger and the E-H-tuner were adjusted for maximum output power. As can be seen from Figure 8a and 8b, neither output power nor efficiency saturate up to the highest applied bias currents. The oscillation frequency varies only slightly and is mainly determined by the resonant cap. An output power of 33 mW at 93.5 GHz with an efficiency of 2.65 % and an output power 31.5 mW at 107.36 GHz with an efficiency of 3.35 % were obtained. The highest oscillation frequency of another diode was 112.5 GHz with an output power of 16 mW and the corresponding efficiency of 2.55 %. Table 2 summarizes the experimental results obtained from the so far best diodes. The operating junction temperature was well below $T_j = 550$ K in each case.

Frequency [GHz]	87.22	93.50	102.66	107.30	112.50
Output power [mW]	27	33	33	31.5	16
Efficiency [%]	1.75	2.65	3.35	3.35	2.55

Table 2: Experimental results of TUNNETT diodes in W-band cavities

A plot of the output power and efficiency of the W-band diodes that have been mounted and tested to date is given in Figure 9. There appears to be a broad peak in the RF output power and DC to RF conversion efficiency around the nominal design frequency of 100 GHz. This peak confirms that the first order design rules accurately predict the operating frequency of the TUNNETT diodes. It also indicates that the high field, high temperature electron average drift velocity in GaAs TUNNETT diodes is close to 4.6×10^6 cms^{-1}. The power levels and efficiencies above 100 GHz are comparable to the ones obtained from Gunn devices in this frequency range [20-22].

To verify the mode of operation the DC I-V characteristics are measured at room temperature (T = 300 K) and elevated temperatures (T = 470 K). The I-V curves of a 25 μm diameter W-band TUNNETT diode shown in Figure 10 clearly demonstrate that the injection mechanism is predominantly tunneling. For comparison the I-V curves of a 55 μm V-band MIxed Tunneling and Avalanche Transit-Time (MITATT) diode are also given in Figure 10. At room temperature the MITATT diode has a sharp increase in current at about 18 V due to the onset of impact ionization [16]. The TUNNETT diode I-V curve at room temperature exhibits no sign of this behavior. Tunneling as the dominant breakdown mechanism also explains the temperature dependence of the TUNNETT diode I-V curves. Increasing the junction temperature of the device enhances tunneling and suppresses impact ionization as can be seen in the temperature behavior of the MITATT diode. For low bias voltages the current increases, thus indicating tunneling. The voltage for the sharp increase in current has a positive temperature coefficient, characteristic of impact ionization as previously shown in Figure 6. For the range of applied bias voltages the current in the TUNNETT diode always increases as a function of temperature implying that impact ionization is not significant.

Figure 11 shows the measured spectra of a free running W-band IMPATT diode oscillator with 42.8 mW at 89.2 GHz (Figure 11a) and a free running W-band TUNNETT diode oscillator with 9.2 mW at 92.2 GHz (Figure 11b). and proves that the oscillations have clean spectra. The spectrum of another free running TUNNETT diode oscillator in Figure 12 was taken using the same settings (vertical scale, scan width and resolution bandwidth) of the spectrum analyzer as in Reference 23 for an free running InP Gunn device oscillator and it compares favorably to the spectrum of this Gunn device oscillator.

6. Device simulation

In order to determine the capabilities of GaAs IMPATT diodes at D-band frequencies and in order to find an explanation for the significant decrease in output power above 110 GHz, the device structures were simulated using two IMPATT diode simulation programs, a drift-diffusion (DD) model [24] and an energy-momentum (EM) model [25]. Table 3 shows calculated output power and efficiency at f = 95 GHz as preliminary results for both programs. The data for the device area A_D and current density J_{DC} are

taken from Reference 3. The energy-momentum program shows slightly higher breakdown voltages and higher efficiency and output power. If a series resistance $R_s = 0.18\ \Omega$ is taken into account for this diode, the calculated output power and efficiency are much closer to the measured values. This series resistance is comparable to the value obtained from small signal impedance measurements in forward direction at 32 MHz [9,10].

W-band IMPATT diode

Frequency: 95 GHz Area A_D: 8×10^{-6} cm^2 Current density: 50 kAcm^{-2}

Model	Voltage	Power ($R_s = 0\ \Omega$)	Efficiency	Power ($R_s = 0.18\ \Omega$)	Efficiency
	[V]	[mW]	[%]	[mW]	[%]
DD	12.2	550	11.3	320	6.5
EM	12.5	700	14.0	510	10.2

D-band IMPATT diode

Frequency: 140 GHz Area A_D: 5×10^{-6} cm^2 Current density: 60 kAcm^{-2}

Model	Voltage	Power ($R_s = 0\ \Omega$)	Efficiency	Power ($R_s = 0.20\ \Omega$)	Efficiency	Power ($R_s = 0.288\ \Omega$)	Efficiency
	[V]	[mW]	[%]	[mW]	[%]	[mW]	[%]
DD	10.4	120	3.8	35	1.1	12	0.4
EM	10.9	215	6.5	80	2.4	18	0.5

Table 3: Calculated results for GaAs single-drift flat-profile IMPATT diodes.

The results for the D-band structure in Table 3 were calculated for no series resistance and two different values of the series resistance. $R_s = 0.288\ \Omega$ assumes that the series resistance is mainly due to the contact resistances of the p^+ and n^+ layers and scales with reciprocal area, i.e. it is equivalent to $R_s = 0.18\ \Omega$ of the W-band diode. For this series resistance the output power is reduced to about one tenth of the output

power for the case of no series resistance taken into account. Since the calculated output power agrees with the experimental value of 9 mW at 128.4 GHz, the series resistance is believed to be the main reason for the significant rolloff in performance above 110 GHz. As can be seen also from Table 3, the output power reduction is only about one third and therefore much less pronounced, if a slightly smaller $R_s \times A_D$ (1×10^{-6} Ωcm^2) is assumed. This demands better technology for contacts on both p^+- and n^+-type GaAs.

Neither the drift-diffusion model nor the energy-momentum model consider any losses in the cavity. These losses are due to the large transformation ratio (up to 500) from the low impedance level between the contacts of the diode and the high impedance level of the waveguide.

The simplified large-signal model for TUNNETT diodes [14] which was employed in the design was also used to determine how strongly the series resistance influences output power and efficiency of these devices. The above mentioned drift velocity v_s and the actual device dimensions (mesa height and diameter, heat sink thickness, etc.) were used for the simulation. In Table 4 the specific contact resistance was assumed to be $\rho_c = 1 \times 10^{-7}$ Ωcm^2 for the p^+ ohmic as well as for the n^+ ohmic contact. In this case the predicted RF output power into a load of $R_l = 1$ Ω is 251 mW for experimentally investigated diameters around 25 μm.

Freq (GHz)	Drift Length (μm)	Drift Field (kV/cm)	V_{DC} (Volts)	V_{RF} (Volts)	V_{DC}/V_{RF}	J_{DC} kA/cm^2
100.0	0.345	309.8	12.29	10.89	0.886	32.84

DIAM (μm)	AREA (μm^2)	R_s (Ohm)	R_d (Ohm)	R_l (Ohm)	V_{RF} (Volt)	I_{DC} (mA)	P_{DC} (W)	P_{RF} (Gen) (mW)	P_{RF} (Load) (mW)
15	177	0.33	2.36	2.02	10.89	58	0.71	134	115
20	314	0.21	1.33	1.12	10.89	103	1.27	238	201
25	491	0.15	1.15	1.00	8.40	161	1.98	287	251
30	707	0.11	1.11	1.00	6.35	232	2.85	313	281

DIAM (μm)	P_{DC} (W)	P_{RF} (mW)	R_{th} (Cu) (°C/W)	R_{th} (Di) (°C/W)	ΔT (Cu) (°C)	ΔT (Di) (°C)
15	0.71	115	213	140	127	84
20	1.26	201	140	86	149	91
25	1.98	251	103	59	178	102
30	2.85	281	80	44	207	113

Table 4: Performance of TUNNETT diodes at 100 GHz for $\rho_c = 1 \times 10^{-7}$ Ωcm^2 and $V_{RF}/V_{DC} \leq 0.886$.

As described above for the IMPATT diodes, present GaAs technology, however, gives a specific contact resistance closer to $\rho_c = 7.5 \times 10^{-7}$ Ωcm². As a result, the RF output power into 1 Ω decreases to 171 mW. For the predicted results in Table 4 and 5 the maximum RF voltage was limited to 88.6 % of the applied DC bias voltage. Since IMPATT diodes at millimeter wave frequencies operate at an RF voltage around or less than 50 % of the DC bias voltage, this case was also investigated for the TUNNETT diodes. As can be seen from Table 6 the RF output power drops to 158 mW for experimentally investigated diameters around 25 µm.

Freq (GHz)	Drift Length (µm)	Drift Field (kV/cm)	V_{DC} (Volts)	V_{RF} (Volts)	V_{DC}/V_{RF}	J_{DC} kA/cm²
100.0	0.345	309.8	12.29	10.89	0.886	32.84

DIAM (µm)	AREA (µm²)	R_s (Ohm)	R_d (Ohm)	R_l (Ohm)	V_{RF} (Volt)	I_{DC} (mA)	P_{DC} (W)	P_{RF} (Gen) (mW)	P_{RF} (Load) (mW)
15	177	1.07	2.36	1.29	10.89	58	0.71	134	73
20	314	0.62	1.62	1.00	9.15	103	1.27	200	124
25	491	0.41	1.41	1.00	7.05	161	1.98	241	171
30	707	0.30	1.30	1.00	5.61	232	2.85	276	213

DIAM (µm)	P_{DC} (W)	P_{RF} (mW)	R_{th} (Cu) (°C/W)	R_{th} (Di) (°C/W)	ΔT (Cu) (°C)	ΔT (Di) (°C)
15	0.71	73	213	140	136	90
20	1.27	124	140	86	160	98
25	1.98	171	103	59	186	107
30	2.85	213	80	44	212	116

Table 5: Performance of TUNNETT diodes at 100 GHz for $\rho_c = 7.5 \times 10^{-7}$ Ωcm² and $V_{RF}/V_{DC} \leq 0.886$.

The calculated values of the thermal resistance R_{th} and temperature rise ΔT for a copper (Cu) or diamond (Di) heat sink are also included in Tables 4, 5 and 6. It should be noted that experimental values for the thermal resistance always are higher than calculated. Therefore, a diode with a diameter of 30 µm on a copper heat sink will be operated at a lower DC input power P_{DC} and therefore reduced RF output power P_{RF} to achieve an operating junction temperature below 250 °C.

Similar to the IMPATT diode simulation, the simplified large-signal TUNNETT diode simulation does not account for any losses due to the large transformation ratio from the low impedance level between the contacts of the diode and the high impedance level of the waveguide. Since the structure of the resonant cap full height waveguide cavity has been optimized for IMPATT diodes its impedance transformation losses are expected to be higher for the TUNNETT diodes.

Freq (GHz)	Drift Length (μm)	Drift Field (kV/cm)	V_{DC} (Volts)	V_{RF} (Volts)	V_{DC}/V_{RF}	J_{DC} kA/cm^2
100.0	0.345	309.8	12.29	10.89	0.500	32.84

DIAM (μm)	AREA (μm^2)	R_s (Ohm)	R_d (Ohm)	R_l (Ohm)	V_{RF} (Volt)	I_{DC} (mA)	P_{DC} (W)	P_{RF} (Gen) (mW)	P_{RF} (Load) (mW)
15	177	1.07	4.63	3.56	6.14	58	0.71	76	58
20	314	0.62	2.61	1.99	6.14	103	1.27	134	103
25	491	0.41	1.67	1.26	6.14	161	1.98	210	158
30	707	0.30	1.30	1.00	5.61	232	2.85	276	213

DIAM (μm)	P_{DC} (W)	P_{RF} (mW)	R_{th} (Cu) (°C/W)	R_{th} (Di) (°C/W)	ΔT (Cu) (°C)	ΔT (Di) (°C)
15	0.71	58	213	140	136	90
20	1.27	103	140	86	162	98
25	1.98	158	103	59	186	107
30	2.85	213	80	44	212	116

Table 6: Performance of TUNNETT diodes at 100 GHz for $\rho_c = 7.5 \times 10^{-7}$ Ωcm^2 and $V_{RF}/V_{DC} \leq 0.50$.

7. Conclusions

The experimental results clearly show that GaAs IMPATT diodes are powerful devices not only for frequencies below 60 GHz, but also above 100 GHz. The predicted results of two different simulation programs agree with the experiment. These simulations also reveal that the contact technology is very crucial for high output power and efficiency and must be improved considerably for GaAs D-band IMPATT diodes. The results from D-band GaAs IMPATT diodes and from W-band GaAs TUNNETT diodes are the best reported to date. Both IMPATT and TUNNETT diodes exhibit clean spectra for local oscillator applications. The TUNNETT diodes demonstrate useful power levels and efficiencies comparable to Gunn devices. Since RF output power and DC to RF conversion efficiency do not saturate up to the highest applied DC bias currents, still higher output power levels and efficiencies can be expected from TUNNETT diodes on diamond heat sinks in optimized cavities.

References

[1] Elta, M. E., Fettermann, H. R., Macropoulos, W. V., and Lambert, J.: "150 GHz GaAs MITATT source", *IEEE Electron Device Letters*, **EDL-1**, 1980, pp. 115-116.

[2] Chang, K., Kung, J. K., Asher, P. G., Hayashibara, G. M., and Ying, R. S.: "GaAs Read-type IMPATT diode for 130 GHz CW operation", *Electronics Letters*, **17**, 1981, pp. 471-473.

[3] Eisele, H., and Grothe, H.: "GaAs W-band IMPATT diodes made by MBE", *Proc. MIOP '89*, Sindelfingen, FRG, Feb. 28th - March 3rd 1989, Session 3A.6.

[4] Eisele, H.: "GaAs W-band IMPATT diodes for very low-noise oscillators", *Electronics Letters*, **26**, 1990, pp. 109-110.

[5] Nishizawa, J., Motoya, K., and Okuno, Y.: "Submillimeter Wave Oscillation from GaAs TUNNETT Diode", *Proceedings of the 9th European Microwave Conference*, 1979, pp. 463-467.

[6] Pöbl, M., Freyer, J.: "Characterization of W-Band CW TUNNETT Diode", *Proceedings of the 21st European Microwave Conference*, Stuttgart, FRG, 1991, pp. 1496-1501.

[7] Kwon, Y., Pavlidis, D., Tutt, M., Ng, G. I., Lai, R., and Brock, T.: "W-Band Monolithic Oscillator Using InAlAs/InGaAs HEMT's", *Electronics Letters*, **26**(18), 1990, pp. 1425-1426.

[8] Rolland P. A., Friscourt M. R., Lippens D., Dalle C., and Nieruchalski, J. L.: "Millimeter Wave Solid-State Power Sources", *Proceedings of the International Workshop on Millimeter Waves*, Rome, Italy, April 2-4, 1986, pp. 125-177.

[9] Eisele, H.: "Electron properties in GaAs for the design of mm-wave IMPATTs", *International Journal of Infrared and Millimeter Waves*, **4**, 1991, pp. 345-354.

[10] Eisele, H.: "GaAs W-Band IMPATT diodes: The first step to higher frequencies", *Microwave Journal*, **34**, 1991, pp. 275-282.

[11] Okuto, Y., and Crowell, C. R., "Threshold energy effects on avalanche breakdown voltage in semiconductor junctions", *Solid-State Electronics*, **18**, 1975, pp. 161-168

[12] Hulin, R.: "Großsignalmodell von Lawinenlaufzeitdioden", Ph.D. Thesis Techn. University Braunschweig, Braunschweig, 1973.

[13] Harth., W., Claassen, M.: "Aktive Mikrowellendioden", Springer-Verlag, Berlin, 1981.

[14] Haddad, G. I., East, J. R., and Kidner, C.: "Tunnel Transit-Time (TUNNETT) Devices for Terahertz Sources", *Microwave and Optical Technology Letters*, **4**, 1991, pp. 23-29.

[15] Allam, R., and Pribetich, J.: "Temperature Dependence of Electron Saturation Velocity in GaAs", *Electronics Letters*, **26**, 1990, pp. 688-689.

[16] Kidner, C., Eisele, H., and Haddad, G. I.: "Tunnel Injection Transit-Time Diodes for W-Band Power Generation", *Electronics Letters*, **28**, 1992, pp. 511-513.

[17] Kidner, C., Eisele, H., East, J., and Haddad, G. I.: "Design, Fabrication and Evaluation of Tunnel Transit-Time Diodes for V-Band and W-Band Power Generation", to be presented at the *1992 IEEE MTT-S International Microwave Symposium*, June 1 - June 5, 1992, Albuquerque, New Mexico.

[18] Eisele, H.: "Selective etching technology for 94 GHz GaAs IMPATT diodes on diamond heat sinks", *Solid-State Electronics*, **32**, 1989, pp. 253-257.

[19] Kamoua, R., Eisele, H., East, J. R., Haddad, G. I., Munns, G., Sherwin, M.: "Modeling, Design, Fabrication, and Testing of InP Gunn Devices in the D-Band (110 GHz - 170 GHz), these *Proceedings of the 3rd International Symposium on Space Terahertz Technology*, March 24-26, 1992, Ann Arbor, Michigan.

[20] Wandinger, L.: "mm-Wave InP Gunn Devices: Status and Trends", *Microwave Journal.*, **24**(3), 1981, pp. 71-78.

[21] Eddison, I. G., et al.: "Efficient fundamental frequency oscillation from mm-wave InP n^+-n-n^+ TEOs", *Electronics Letters*, **17**(20), 1981, pp. 758-760.

[22] Teng, S. J. J., Goldwasser, R. E.: "High Performance Second-Harmonic Operation W-Band GaAs Gunn Diodes", *IEEE Electron Device Letters*, **EDL-10**(9), 1989, pp. 412-414.

[23] Perrin, O., et al.: "380 GHz Receiver Front-End for the Balloon-Borne Radioastronomical Experiment", *Proceedings of the 2nd International Symposium on Space Terahertz Technology*, February 26-28, 1991, Pasadena, California, pp. 622-640.

[24] Bauhahn, P. E., and Haddad, G. I.: "IMPATT device simulation and properties", *IEEE Transactions on Electron Devices*, **ED-24**, 1977, pp. 634-642.

[25] Mains, R. K., Haddad, G. I., and Blakey, P. A.: "Simulation of GaAs IMPATT Diodes Including Energy and Velocity Transport Equations", *IEEE Transactions on Electron Devices*, **ED-30**, 1983, pp. 1327-1338.

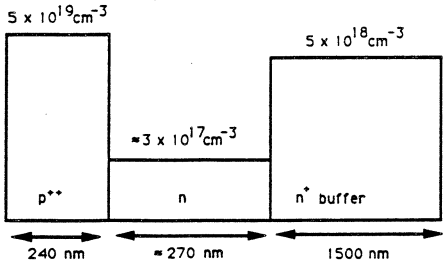

Fig. 1: Nominal device structure of a GaAs D-band single-drift flat-profile IMPATT diode.

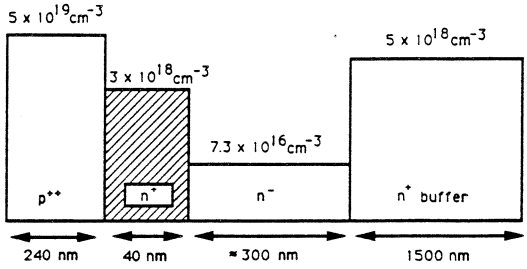

Fig. 2: Nominal device structure of a GaAs W-band single-drift TUNNETT diode.

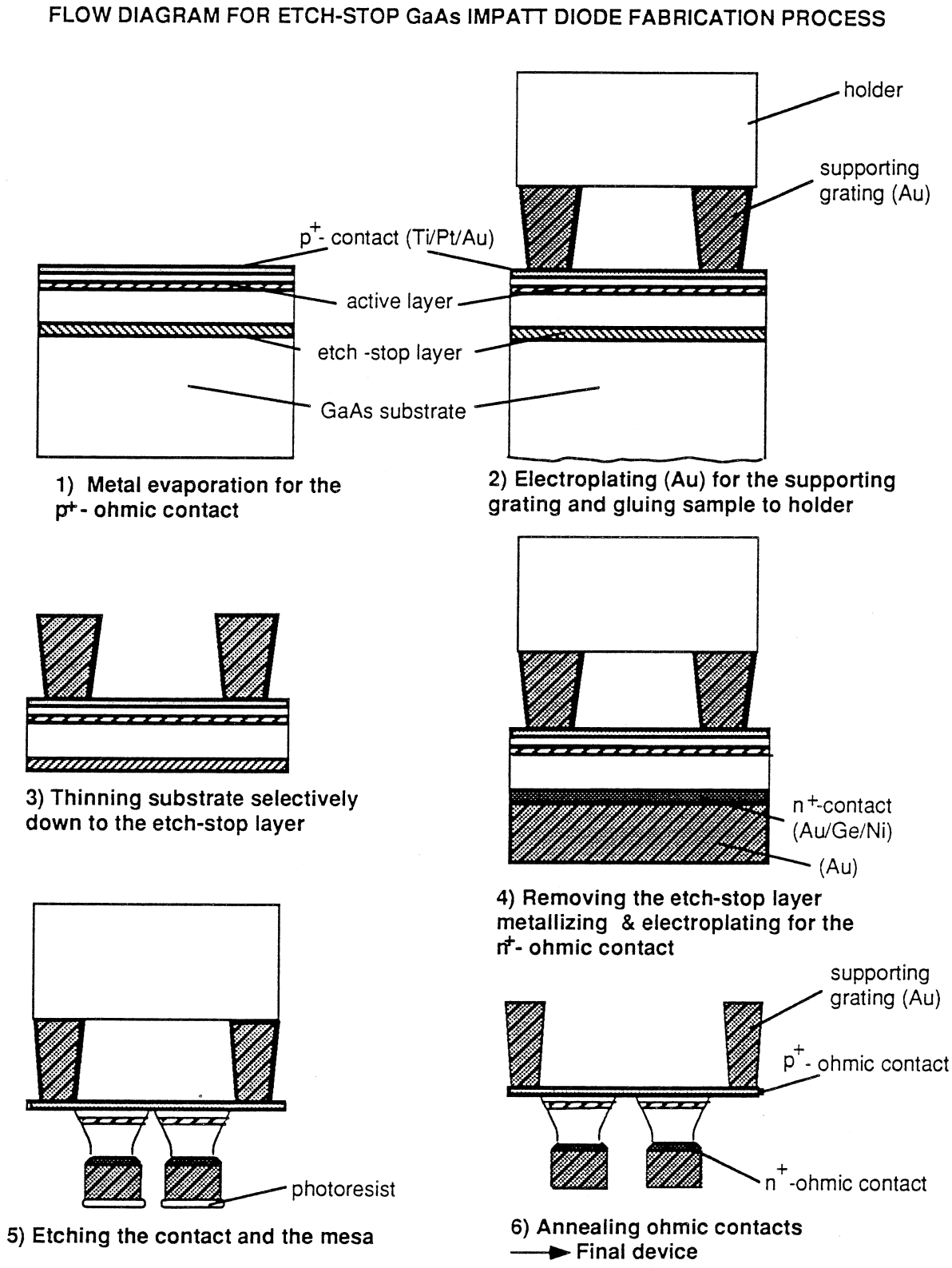

Fig. 3: Flow chart for IMPATT diodes device fabrication.

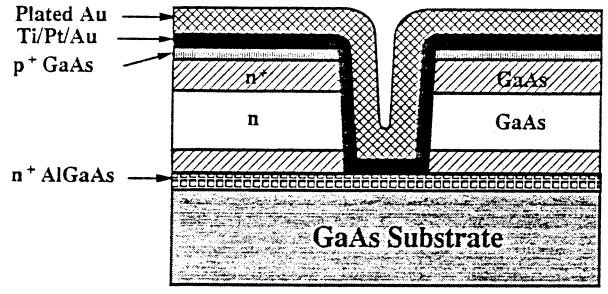

a) Island definition, p-ohmic evaporation, and gold plating (~ 15 μm)

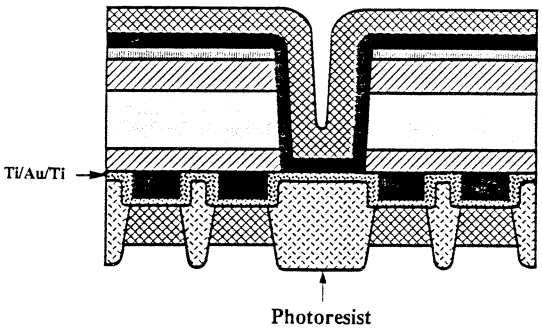

c) Gold plating of ohmic contacts

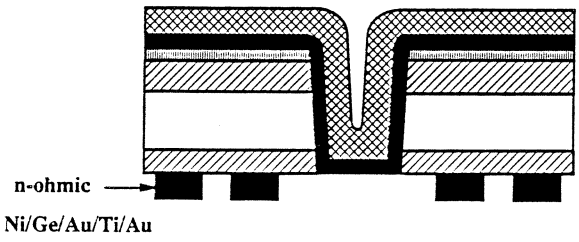

b) Substrate thinning, etch stop layer removal, and n-ohmic evaporation

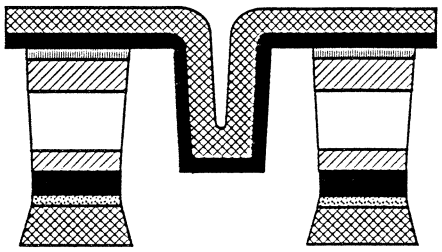

d) Final diodes after annealing and mesa etch

Fig. 4: Flow chart for TUNNETT diodes device fabrication.

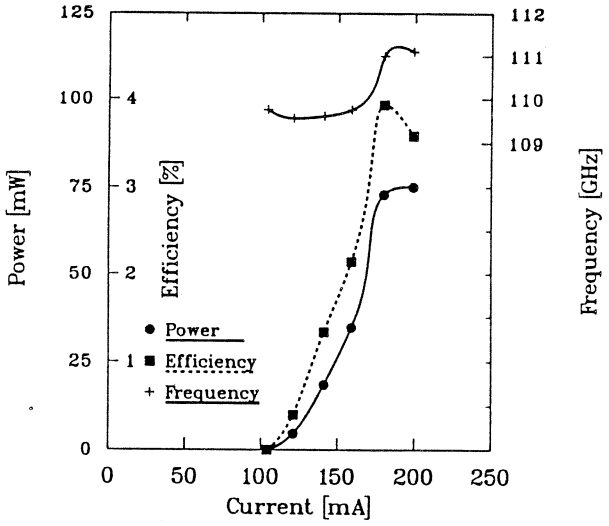

Fig. 5: Output power, efficiency and oscillation frequency as a function of bias current for a GaAs single-drift flat-profile IMPATT diode.

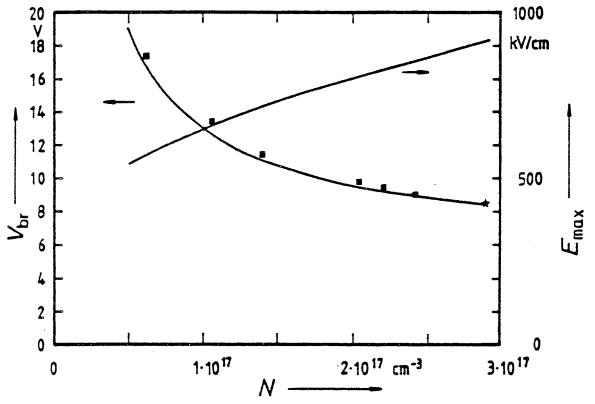

Fig. 7: Breakdown voltage V_{br} and peak electric field E_{max} of an abrupt p⁺n-junction.
■ ★ : measured
—— : calculated.

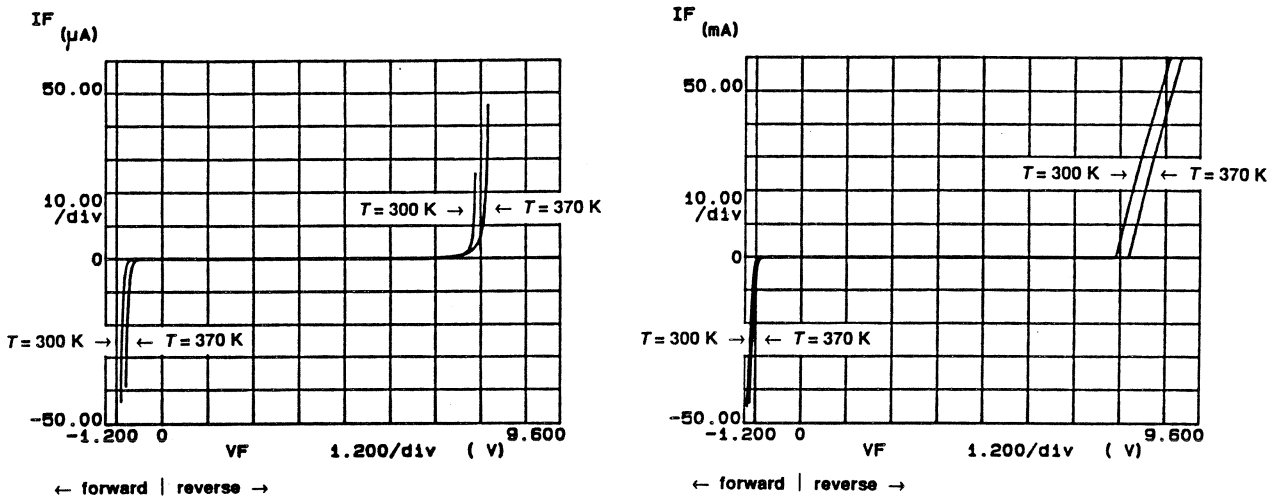

(a) (b)

Fig. 6: Current-voltage characteristics of a GaAs single-drift flat-profile IMPATT diode at room temperature (300 K) and an elevated temperature (370 K).

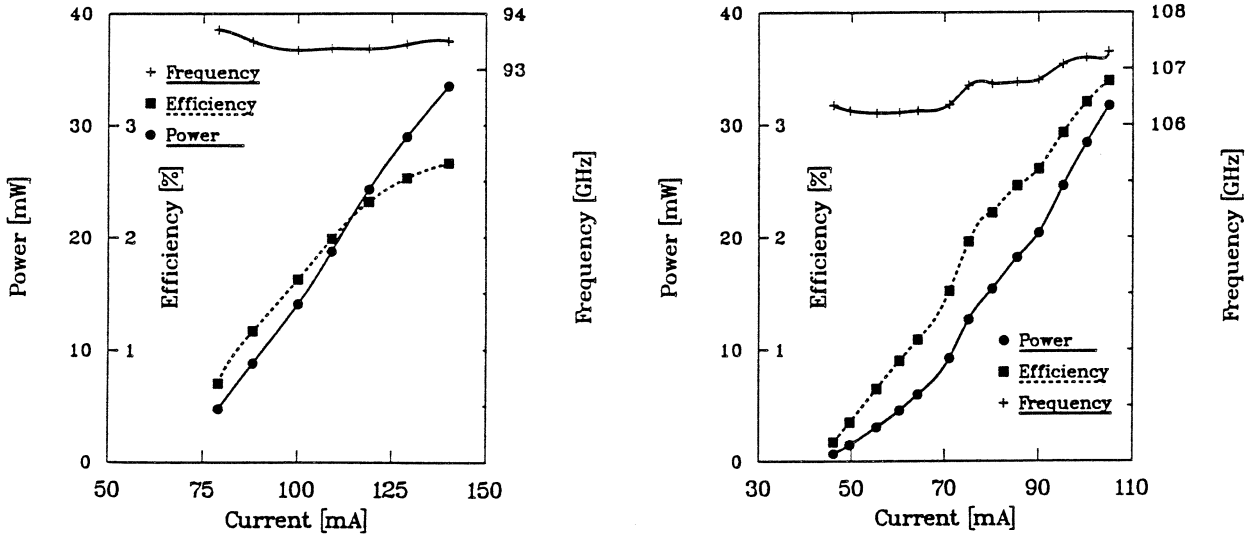

(a) (b)

Fig. 8: Output power, efficiency and oscillation frequency as a function of bias current for two W-band GaAs single-drift TUNNETT diodes.

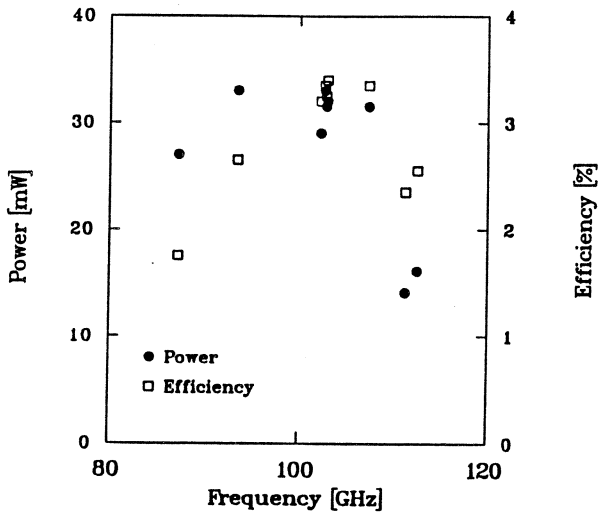

Fig. 9: Output power and efficiency of GaAs single-drift TUNNETT diodes in W-band.

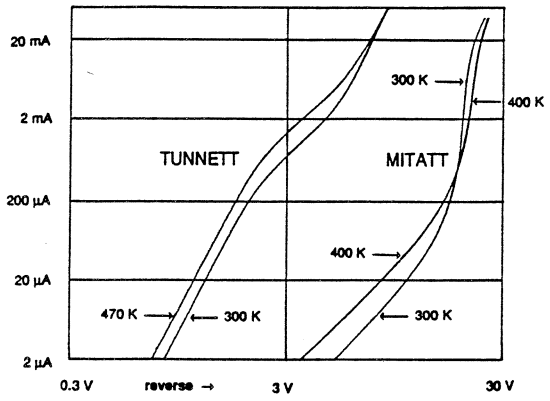

Fig. 10: Reverse bias current-voltage characteristics for pure tunnel injection (TUNNETT) and mixed tunnel injection and impact ionization (MITATT) at room temperature (300 K) and elevated temperatures (470 K and 400 K, respectively).

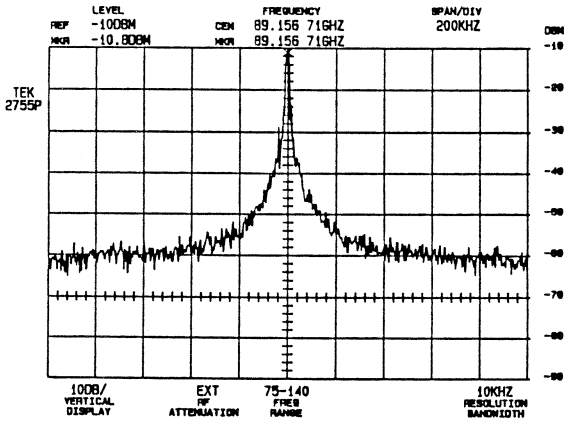

(a)

Fig. 11: Spectrum of a W-band IMPATT diode free running oscillator, power level 42.8 mW, center frequency 89.16 GHz, vertical scale 10 dB/div, horizontal scale 200 kHz/div, BW 10 kHz.

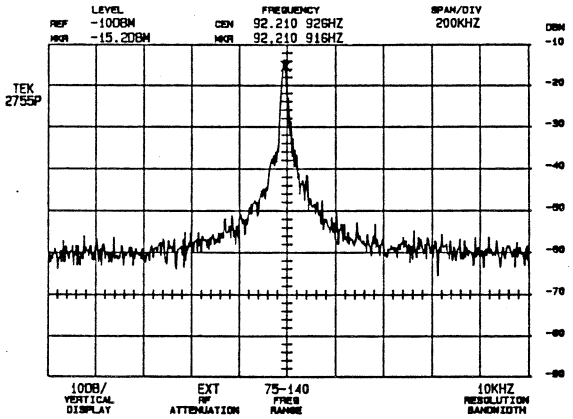

(b)

Fig. 11: Spectrum of a W-band TUNNETT diode free running oscillator, power level 9.2 mW, center frequency 92.21 GHz, vertical scale 10 dB/div, horizontal scale 200 kHz/div, BW 10 kHz.

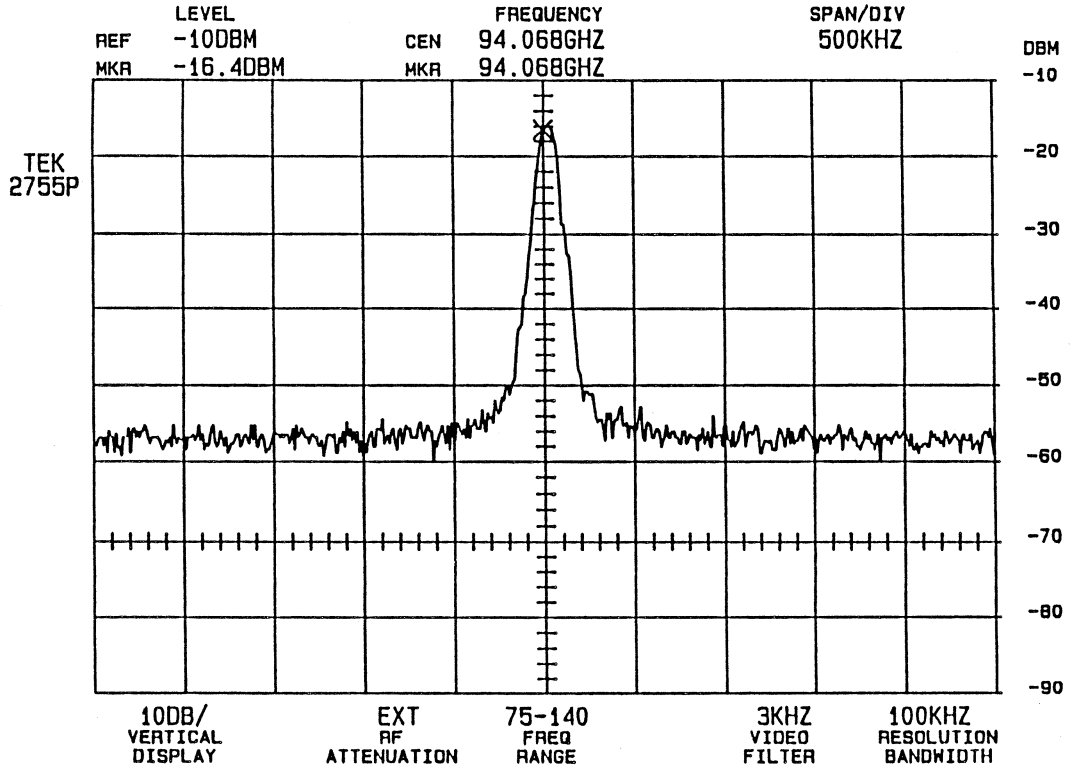

Fig. 12: Spectrum of a W-band TUNNETT diode free running oscillator, power level 8.8 mW, center frequency 94.07 GHz, vertical scale 10 dB/div, horizontal scale 500 kHz/div, BW 100 kHz.